The Astronomical Journal, 127:2659–2673, 2004 May

CHANDRA X-RAY OBSERVATIONS OF YOUNG CLUSTERS. I. NGC 2264 DATA

Solange V. Ramírez,[1] Luisa Rebull,[1] John Stauffer,[1] Thomas Hearty,[2] Lynne Hillenbrand,[3] Burton Jones,[4] Russell Makidon,[5] Steven Pravdo,[2] Steven Strom,[6] and Michael Werner[2]

Received 2003 October 24; accepted 2004 January 23

ABSTRACT

We present results of a *Chandra* observation of a field in NGC 2264. The observations were taken with the ACIS-I camera with an exposure time of 48.1 ks. We present a catalog of 263 sources, which includes X-ray luminosity, optical and infrared photometry, and X-ray variability information. We found 41 variable sources, 14 of which have a flarelike light curve, and two of which have a pattern of a steady increase or decrease over a 10 hr period. The optical and infrared photometry for the stars identified as X-ray sources are consistent with most of these objects being pre–main-sequence stars with ages younger than 3 Myr.

Key words: stars: activity — stars: pre–main-sequence — X-rays: stars

On-line material: machine-readable tables

1. INTRODUCTION

NGC 2264 is a cluster of young stars, part of the Mon OB1 association. It is about 3 Myr old (Park et al. 2000), and the shape of its initial mass function is very similar to that of Orion (Sung et al. 1997). Pre–main-sequence (PMS) stars have been identified in NGC 2264 using a variety of methods, including Hα spectroscopy (Herbig 1954; Ogura 1984), Hα narrowband photometry (Sung et al. 1997; Park et al. 2000), irregular variability (Adams et al. 1983), near-IR photometry (Lada et al. 1993), proper motions (Vasilevskis et al. 1965), and X-ray flux (Flaccomio et al. 2000; Patten et al. 1994; Simon et al. 1985). Furthermore, several techniques have been used to identify circumstellar disk candidates, including excess ultraviolet ($U-V$) emission, excess near-IR ($I-K$ and $H-K$) emission, and Hα emission-line equivalent widths (e.g., Rebull et al. 2002). Rebull et al. (2002) have found a good correlation between disk indicators and report lower limits for the disk fraction ranging from 21% to 56%. They also found a typical value for mass accretion rates of $\sim 10^{-8}\ M_{\odot}\ \mathrm{yr}^{-1}$, comparable to the values derived for Orion and Taurus-Auriga.

NGC 2264 provides a laboratory for studying the interrelationships of rotation, mass accretion, disk indicators, and X-ray luminosity of PMS stars. The question of how exactly these things are related is still an open problem in star formation phenomenology. There is a clear relationship between rotation rate (period) and X-ray luminosity (L_X) found in late-type stars in clusters as old as NGC 2547 (15–40 Myr; Jeffries et al. 2000) through the Hyades ($\sim$500 Myr; Stauffer et al. 1997). The ratio between the X-ray and bolometric luminosity, L_X/L_{bol}, increases with increasing rotation rate, until the most rapidly rotating stars reach a maximum X-ray luminosity (or saturation level) such that $L_X/L_{bol} \sim 10^{-3}$ (see Pizzolato et al. 2003 and references therein). It is much less clear that rotation and L_X/L_{bol} are related in younger clusters (e.g., Gagne et al. 1995). Feigelson et al. (2003) see no obvious correlation between rotation and L_X/L_{bol} for their Orion ($\sim$1 Myr old; Hillenbrand 1997) sample and conclude that the X-ray generation mechanism for young PMS stars must be different from that responsible in young main-sequence stars. Flaccomio et al. (2003) analyze data for a number of young associations and clusters (including Orion), and agree that there is little correlation between L_X/L_{bol} and rotation at very young ages, but conclude that the data are consistent with a single physical mechanism, by which the Orion-age stars are simply all at or near the saturation level (and that level and the critical velocity for it are a function of gravity/age). We want to study at what age the relationship between rotation and L_X/L_{bol} emerges. NGC 2264 ($\sim$3 Myr old; Sung et al. 1997; Park et al. 2000), being slightly older than Orion, is at an ideal age to probe the relationship between these parameters.

Chandra observations provide a unique tool to improve the X-ray sample of PMS stars in NGC 2264. The high spatial resolution provided by the ACIS camera allows us to resolve the source confusion present in previous *ROSAT* data samples. The *Chandra* sensitivity extends the X-ray flux limit from the *ROSAT* value of $\log L_X(\mathrm{ergs\ s^{-1}}) \sim 30.1$ to $\log L_X(\mathrm{ergs\ s^{-1}}) \sim 28.5$, allowing us to detect lower mass stars and explore the mass dependence of the rotation and L_X relationship.

In the present paper, we present results of *Chandra* observations of NGC 2264. We discuss source detection, variability and L_X determination, providing a catalog of 263 X-ray sources. In Paper II (Rebull et al. 2004), we will discuss in more detail the relationships found here between rotation rate, mass accretion rate, disk indicators, and X-ray luminosity. We rely heavily on data from our earlier papers on this cluster, Rebull et al. (2002) and Makidon et al. (2004), providing optical photometry and periods, respectively.

2. OBSERVATIONS

NGC 2264 was observed with the Advanced CCD Imaging Spectrometer (ACIS) detector on board the *Chandra X-Ray Observatory* (Weisskopf et al. 2002) on 2002 February 9. The

[1] *Spitzer* Science Center, MS 220-06, California Institute of Technology, Pasadena, CA 91125.
[2] Jet Propulsion Laboratory, California Institute of Technology, 4800 Oak Grove Drive, Pasadena, CA 91109.
[3] Department of Astronomy, MS 105-24, California Institute of Technology, Pasadena, CA 91125.
[4] Department of Astronomy and Astrophysics, University of California, Santa Cruz, 1156 High Street, Santa Cruz, CA 95064.
[5] Space Telescope Science Institute, 3700 San Martin Drive, Baltimore, MD 21218.
[6] Kitt Peak National Observatory, NOAO, 955 North Cherry Avenue, Tucson, AZ 85719.

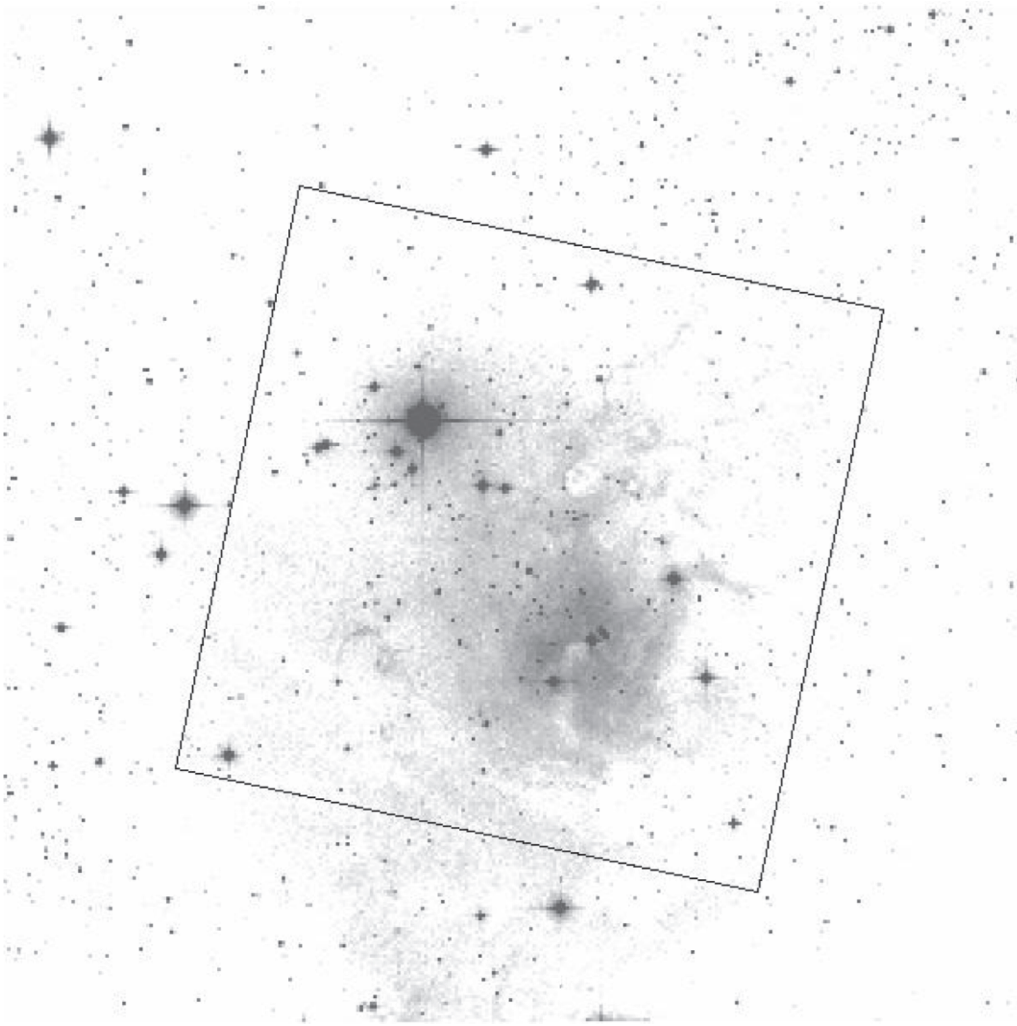

FIG. 1.—Image of NGC 2264 from the Palomar Digital Sky Survey (Reid et al. 1991). The image has a field of view of $30' \times 30'$, and the box represents the field of view of the *Chandra* ACIS-I observations, centered at R.A. = $6^h40^m48^s$, decl. = $+9°51'$ (J2000.0).

results presented here arise from the imaging array (ACIS-I), which consists of four 1024×1024 front-side illuminated CCDs. The array is centered at $6^h40^m48^s$, $+9°51'$ and covers an area on the sky of about $17' \times 17'$. Figure 1 shows a $30' \times 30'$ image of NGC 2264 from the Palomar Digital Sky Survey (Reid et al. 1991), with the *Chandra* ACIS-I field of view marked as a box. The field was selected to maximize the number of stars in the field of view with known periods from Makidon et al. (2004) and with minimal overlap with another contemporaneous *Chandra* NGC 2264 observation (Flaccomio et al. 2003). The total exposure time of the ACIS observations is 48.1 ks.

2.1. *Data Preparation*

We started data analysis with the Level 1 processed event list provided by the pipeline processing at the *Chandra* X-Ray Center. We have kept all events, including the ones flagged as cosmic-ray afterglows by the pipeline. The presence of spurious sources due to cosmic-ray afterglows was eliminated using the light curves of the detected sources (see § 3.3). The energy and grade of each data event were corrected for charge transfer inefficiency (CTI), applying the algorithm code described by Townsley et al. (2000). Then the event file was filtered by ASCA grades (keeping grades 0, 2, 3, 4, and 6), by time intervals, and by background flaring due to solar activity. Removal of the background flares identified by the latter step reduced the exposure time to 47.4 ks. The filtering process was done using the *Chandra* Interactive Analysis of Observations (CIAO) package[7] and following the Science Threads[8] provided by the *Chandra* X-Ray Center. Finally, the energy range was restricted to 0.3–10 keV. Figure 2 shows the ACIS-I image of the filtered observations.

2.2. *Source Detection*

The CIAO package provides three source detection tools, as part of the DETECT software.[9] The CELLDETECT tool uses a sliding square cell to search for statistically significant enhancements over the background. This tool has been widely used with *Einstein* and *ROSAT* data, and works well in the detection of faint sources outside crowded fields. The VTPDETECT tool determines individual densities for every occupied pixel and analyzes the distribution of densities for significant source enhancements. This tool works well in the

[7] See http://cxc.harvard.edu/ciao/index.html.
[8] See http://cxc.harvard.edu/ciao/threads/index.html.
[9] See http://cxc.harvard.edu/ciao/download/doc/detect_html_manual.

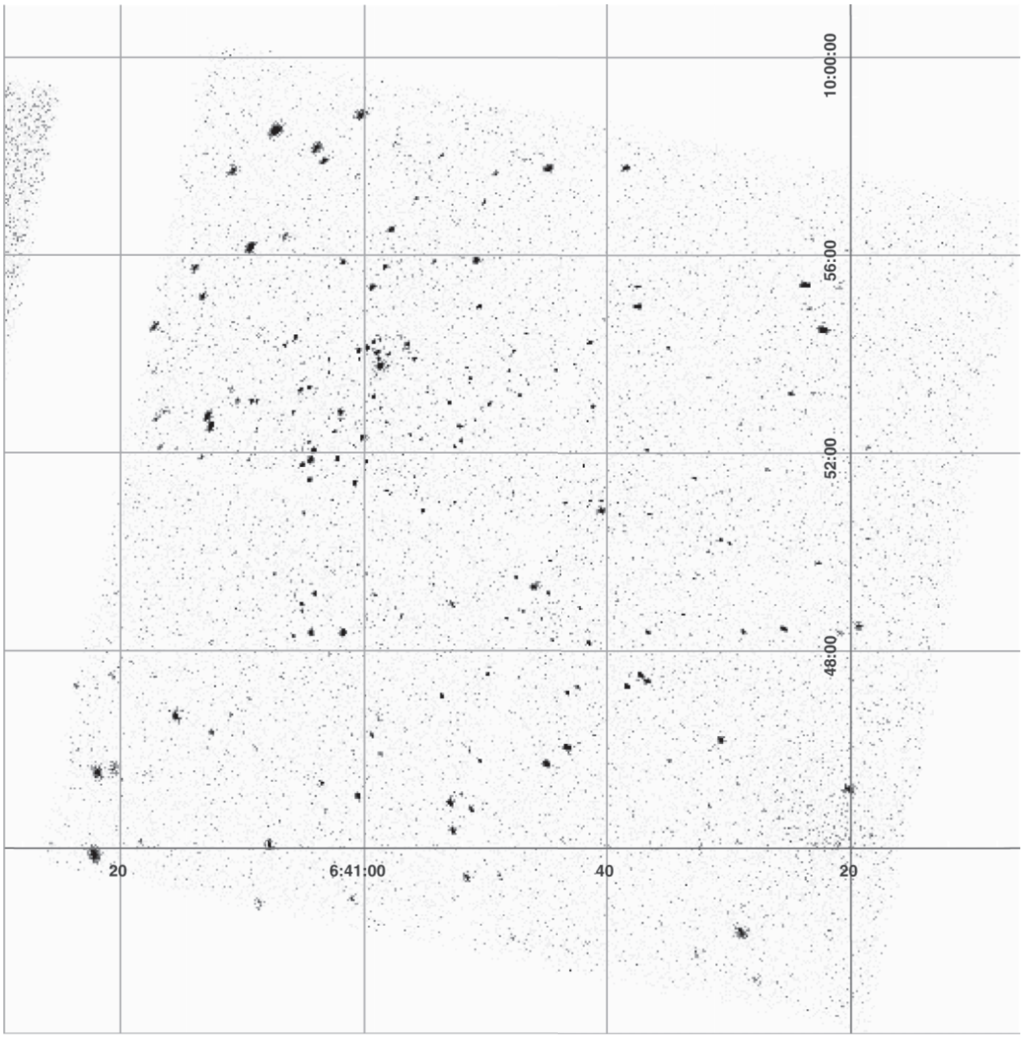

FIG. 2.—Image of NGC 2264, observed with the *Chandra* ACIS-I. The image has a field of view of $17' \times 17'$, and it is centered at R.A. = $6^h40^m48^s$, decl. = $+9°51'$ (J2000.0). This image contains only filtered events.

detection of low surface brightness features, but combines closely spaced point sources. The WAVDETECT tool performs a Mexican hat wavelet decomposition and reconstruction of the image and then searches for significant correlations. This tool works well in separating closely spaced point sources. We chose the WAVDETECT tool to determine the X-ray sources in our *Chandra* observations, since it is the tool that properly handles crowded fields like ours. The algorithm used by WAVDETECT is described in Freeman et al. (2002). We used wavelet scales ranging from 1 to 16 pixels in steps of $\sqrt{2}$, and the default source significance threshold of 1×10^{-6}. The WAVDETECT tool was run separately in the four ACIS-I CCD images, and it produced an original list of 313 sources (see § 3.1).

2.3. *Astrometric Alignment*

The positions of the sources obtained by WAVDETECT were correlated with I_C-band positions (Rebull et al. 2002) from the optical/infrared catalog of NGC 2264 stars compiled for our project (see the description of the catalog in § 4.1). Each X-ray source was manually checked to confirm that the optical/infrared counterpart lay within the radius for count extraction (defined in § 3.1). We checked the astrometry of the *Chandra* observations using all X-ray sources located within an off-axis angle (ϕ) less than 5′ that have I_C-band counterparts from Rebull et al. (2002). A total of 80 sources meet this criteria. We determined a mean offset in right ascension of $-0\overset{''}{.}74 \pm 0\overset{''}{.}20$ and a mean offset in declination of $0\overset{''}{.}14 \pm 0\overset{''}{.}20$ between the *Chandra* and I_C-band coordinates. Figure 3 shows the coordinate offsets of the 80 sources within $\phi < 5'$ and with I_C-band counterparts. The mean offset is marked by a plus sign. The *Chandra* positions were corrected by these mean offsets so that the X-ray sources fall in the same reference frame as their optical counterparts.

3. RESULTS

3.1. *X-Ray Photometry*

X-Ray aperture photometry was initially performed on the 313 sources detected by the CIAO tool WAVDETECT. The radius for count extraction, $R_{\rm ext}$, is different for each source, given the variation of the point spread function (PSF) across the field. Feigelson et al. (2002) defined the 95% and 99% encircled energy radii [R(95%EE) and R(99%EE)], as a function of off-axis angle (ϕ), in their footnote 12. We set $R_{\rm ext}$ equal to R(95%EE), except for sources with higher than 1000 counts, where we enlarged $R_{\rm ext}$ to be equal to R(99%EE). The X-ray counts ($C_{\rm ext}$) were extracted within a circular region of radius

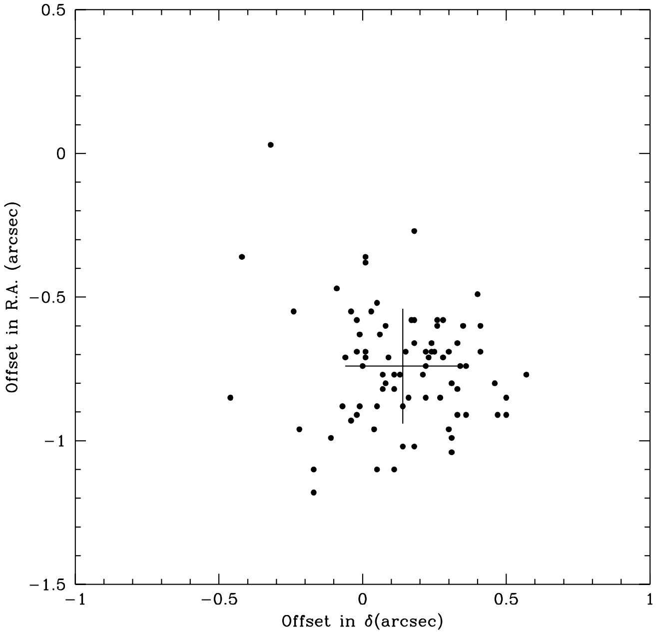

Fig. 3.—Position offsets of 80 X-ray sources, located within $\phi < 5'$, with respect to positions from I_C-band observations. The mean offset in right ascension and declination is marked by a plus sign, the length of which is equal to the standard deviation around the mean right ascension and declination.

$R_{\rm ext}$, using the CIAO tool DMEXTRACT. We also defined an annulus around each source for background determination. The annulus is defined to be between 1.2 R(99%EE) and 1.5 R(99%EE). The background counts were also extracted using the CIAO tool DMEXTRACT. We computed the background in counts per square arcsecond as a function of the off-axis angle (ϕ), performing a 3 σ rejection fit to avoid background counts from annuli that have other sources within them. Indeed, 38 annuli contained detected sources. The computed background was constant as a function of ϕ, and it had a value of $B = (0.063 \pm 0.023)$ counts arcsec^{-2}. The net count, NC, for each source was computed as

$$\mathrm{NC(counts)} = (C_{\rm ext} - B \times \pi R_{\rm ext}^2).$$

To compute the count rate, CR, we also need to determine the enclosed fraction of the PSF, $f_{\rm PSF}$, and the effective exposure time, $t_{\rm eff}$. We computed $f_{\rm PSF}$, using the CIAO tool MKPSF. The effective exposure time is determined from exposure maps, which were generated by the CIAO tool MKEXPMAP. The exposure maps are images of effective area that contain information about instrumental artifacts that are both energy and position dependent. The effective exposure time is the exposure time corrected to account for a 1.3% loss due to readout and scaled to the effective area within $R_{\rm ext}$ with respect to the effective area at the optical axis. The count rate is then computed as

$$\mathrm{CR(counts\ ks^{-1})} = \mathrm{NC}/(f_{\rm PSF} \times t_{\rm eff}).$$

We carefully inspected the light curves of all the sources (see § 3.3) and their appearance in the image of the *Chandra* field of view. A total of 48 (15%) sources were rejected from the original list: 43 sources had light curves consistent with cosmic-ray afterglows, two sources were detected twice, since WAVDETECT was run separately in each CCD, and three sources had net counts less than zero. Of the 43 light curves having a cosmic-ray shape, 40 (93%) contain cosmic-ray afterglows flagged by the pipeline. Our final list of 263 X-ray sources is listed in Table 1.

3.2. *X-Ray Luminosities*

We selected all sources with more than 500 net counts, extracted their spectra and fitted them to measure their X-ray fluxes. A total of 15 sources meeting this criteria are listed in Table 2. The spectra were extracted within $R_{\rm ext}$ using the CIAO tool DMEXTRACT. The spectra of these 15 brightest X-ray sources are shown in Figure 4. The redistribution matrix files (RMFs) and auxiliary response files (ARFs) contain instrument response information that are essential for the spectral fitting process. We use the RMFs provided by the CTI corrector from Townsley et al. (2000). An ARF was created for each source, using the CIAO tool MKARF. The computed ARFs were later corrected to account for the ACIS low-energy quantum efficiency degradation, using the ACISABS absorption model.[10] We used the CIAO tool Sherpa for the spectral fitting. We adopted a photoelectric absorption model (XSWABS), which uses Wisconsin cross sections from Morrison & McCammon (1983). This model has one parameter that is the equivalent hydrogen column density ($N_{\rm H}$). The hydrogen column density was fixed to a value of 0.08×10^{22} cm^{-2} to match an extinction value of $A_V = 0.41$, which is the most likely value of the observed extinction toward NGC 2264, although the A_V can be as high as 3.5 mag (see Rebull et al. 2002 for more discussion). The value of the column density was derived using the relationship of $N_{\rm H} = 2 \times 10^{21} A_V$. If we consider an $N_{\rm H} = 0.65 \times 10^{22}$ cm^{-2}, which corresponds to 3 mag more than the assumed A_V, the derived $L_{\rm X}$ would be only 0.1 dex less. Thus, the error in $L_{\rm X}$ that comes from fixing $N_{\rm H}$ is negligible. We also adopted a thermal emission model (XSMEKAL), which is based on model calculations of Mewe et al. (1985, 1986) and Kaastra (1992), with Fe L calculations by Liedahl et al. (1995). This model includes line emissions from several elements. The remaining two parameters in the model—the plasma temperature (kT) and a normalization factor—were varied in order to fit the spectra.

We initially tried one-temperature models, but they failed to fit the low-energy part of the spectrum. A two-temperature model significantly improved the spectral fitting for all the sources. The brightest X-ray source in the sample 196 (S Mon) has a distinctive soft X-ray spectrum, characteristic of its early spectral type (see § 4.5.1). It also has a high count rate of 155 counts ks^{-1} and may be affected by pileup (at high count rate the observed flux is no longer a linear function of the count rate). Given the spectral characteristics of S Mon and its possible pileup effects, we did not include it in the determination of the conversion factor that leads to the determination of X-ray luminosity for our sample of X-ray sources. The spectral parameters obtained from the two plasma temperature models are listed in Table 2.

The X-ray flux of S Mon listed in Table 2 is the integration of the two-temperature model between 0.3 and 8.0 keV. The X-ray flux for the rest of the bright sources is determined from the best spectral model derived from the mean model parameters. We computed mean plasma temperatures of (0.51 ± 0.06) and (2.5 ± 0.3) keV. The mean plasma temperatures are

[10] See http://cxc.harvard.edu/cal/Acis/Cal_prods/qeDeg/#Obtaining the corrarf and ACISABS tools.

TABLE 1

THE CATALOG OF X-RAY SOURCES

X-Ray ID (1)	Name (2)	R.A. (J2000.0) (3)	Decl. (J2000.0) (4)	ϕ (arcmin) (5)	R_{ext} (arcsec) (6)	f_{PSF} (7)	t_{eff} (ks) (8)	CR (counts ks^{-1}) (9)	Flux (ergs cm^{-2} s^{-1}) (10)	log L_X [log (ergs s^{-1})] (11)	$P_c(\chi^2)$ (%) (12)	Comments[a] (13)
1.................	CXORRS J064009.6+095338	6 40 9.69	9 53 38.355	9.85	14.07	0.99	40.5	0.37	0.228E−14	29.20	100	
3.................	CXORRS J064012.8+094853	6 40 12.84	9 48 53.952	8.78	11.07	0.97	30.2	0.16	0.986E−15	28.83	100	
4.................	CXORRS J064013.5+095313	6 40 13.57	9 53 13.437	8.79	11.12	0.98	42.2	0.21	0.129E−14	28.95	99	
6.................	CXORRS J064018.3+094416	6 40 18.31	9 44 16.054	9.72	13.73	0.99	31.0	0.94	0.579E−14	29.60	100	
8.................	CXORRS J064018.5+095206	6 40 18.57	9 52 6.259	7.34	7.72	0.98	41.9	0.52	0.320E−14	29.35	100	

NOTE.—Table 1 is presented in its entirety in the electronic edition of the Astronomical Journal. A portion is shown here for guidance regarding its form and content. Units of right ascension are hours, minutes, and seconds, and units of declination are degrees, arcminutes, and arcseconds.

[a] Comments: v: variable star; f: flarelike light curve; p: possible flare in the light curve; s: steady increase or decrease in the light curve; g: galaxy.

[b] Flux derived directly from the best-fit model of X-ray spectrum.

TABLE 2
Spectral Properties of Bright Sources

X-Ray ID	Optical ID	CR (counts ks^{-1})	$kT1$ (keV)	$kT2$ (keV)	Flux[a] (10^{-13} ergs cm^{-2} s^{-1})
196	R3295	155.8	0.18	0.57	14.10[b]
113	R2942	84.5	0.30	1.36	5.25
181	R3245	54.9	0.76	3.92	3.45
75	R2752	42.1	0.80	5.16	2.48
94	R2840	36.4	0.40	2.21	2.34
203	R3309	27.4	0.58	2.34	1.68
142	R3091	24.1	1.00	4.46	1.58
251	R3470	21.3	0.34	1.25	1.26
228	R3390	18.5	0.64	2.58	1.04
60	R2633	18.0	0.30	1.66	0.79
208	R3323	17.6	0.25	1.11	1.03
230	R3394	17.2	0.32	1.62	0.95
268	R3555	15.9	0.68	3.28	0.93
16	R2173	14.7	0.41	2.23	0.83
214	R3342	13.3	0.32	2.08	0.76

[a] Flux determined from models of mean plasma temperatures of 0.51 and 2.5 keV; see text.
[b] Flux determined from best-fit model; see text.

held constant, and the integration of the best fit between 0.3 and 8.0 keV provides the X-ray flux. The resulting X-ray fluxes are listed in Table 2.

We use the X-ray fluxes of the 14 bright sources to compute an X-ray flux weighted conversion factor between count rate and X-ray flux. The obtained conversion factor is $(6.16 \pm 0.13) \times 10^{-15}$ (ergs cm^{-2} s^{-1})/(counts ks^{-1}). Figure 5 shows the relationship between CR and X-ray flux for the 14 X-ray sources used to determine the conversion factor. The solid line corresponds to the derived conversion factor. We compiled a list of conversion factors from published studies that were obtained using ACIS-I data in young stars; see Table 3. The values we list for Feigelson et al. (2002) and Getman et al. (2002) were computed using the count rate and X-ray luminosity they provided in their Tables 3 and 1, respectively. Our conversion factor is in good agreement with the ones derived by Krishnamurthi et al. (2001) and Getman et al. (2002), and it differs from the other values by a factor of less than 2. The X-ray flux for our catalog of X-ray sources in NGC 2264, listed in column (10) of Table 1, was computed using the derived conversion factor. The X-ray luminosity, L_X, listed in column (11) of Table 1, is computed assuming a distance to NGC 2264 of 760 pc (Sung et al. 1997).

The limiting luminosity in our X-ray observations varies within the field of view because of the variation of the PSF across the field. In Figure 6, we have plotted the net rate of the detected X-ray sources as a function of the off-axis angle ϕ. The faintest source is located at $\phi \sim 6'$, and it has a count rate of 0.08 counts ks^{-1}, corresponding to an X-ray luminosity of 28.5 at the distance of NGC 2264. About 80% of our sources are located within $\phi = 7'$. At that off-axis angle the limiting count rate has increased to 0.12 counts ks^{-1}, corresponding to an X-ray luminosity of $\log L_X = 28.7$ at the distance of NGC 2264. At $\phi = 10'$, we cannot detect X-ray sources fainter than 0.35 counts ks^{-1} ($\log L_X = 29.2$). Therefore, we adopt a value of $\log L_X = 28.5$ dex as the limiting X-ray luminosity for our observations, keeping in mind that this value holds for sources located within $\phi \sim 6'$.

Flaccomio et al. (2000) observed a $40' \times 100'$ field toward NGC 2264 using *ROSAT*, detecting 169 sources. Our *Chandra* field ($17' \times 17'$) is covered within the spatial extent of the *ROSAT* observations but goes 1.5 dex deeper in log (L_X) (a factor of $\sim$30 in L_X). There are 34 sources in common between our catalog of X-ray sources in NGC 2264 and the *ROSAT* sample of Flaccomio et al. (2000). We compared our X-ray luminosities with the ones given by Flaccomio et al. (2000; see Figure 7). We found a mean difference of –0.1 dex with a standard deviation of 0.3 dex. This difference does not include an offset of +0.3 dex in the *ROSAT* L_X, as described in Flaccomio et al. (2003). Given that many of these PMS stars are highly variable (see § 3.3), we conclude that our luminosities are consistent with respect to those of Flaccomio et al. (2000).

3.3. *Variability*

Light curves were determined for all 313 sources detected by WAVDETECT using the CIAO tool LIGHTCURVES with a bin time of 2500 s. The statistics of the light curves of the sources in our X-ray catalog were obtained using the XRONOS[11] tool LCSTATS. This provides, among other values, the constant source probability as derived from the χ^2 value comparing the data with a constant light curve, $P_c(\chi^2)$. The $P_c(\chi^2)$ values are listed in column (12) of Table 1. The light curves of the sources with $P_c(\chi^2) < 90\%$ were analyzed further, since they are the most likely to be variable. We obtained the reduced χ^2 of those sources, using two additional light curves with bin times of 5000 s and 7500 s. If the reduced χ^2 values obtained for both bin times was less than 2.5, then we consider those sources to have constant light curves. Then we defined variable sources as those having 2500 s bin light curves with $P_c(\chi^2) < 90\%$, and those having 5000 and 7500 s bin light curves with reduced $\chi^2 > 2.5$. There are 41 variable sources that meet these criteria. Variable sources are marked with a "v" in column (13) of Table 1. Among the variable sources, 10 have known periods from Makidon et al. (2004), but we find no obvious dependence of X-ray flux with rotational phase for nine of these stars (see below the discussion about source 181). There are 14 variable sources that show a flare shape, defined as a rapid increase and a slow decrease in

[11] See http://heasarc.gsfc.nasa.gov/docs/xanadu/xronos/xronos.html.

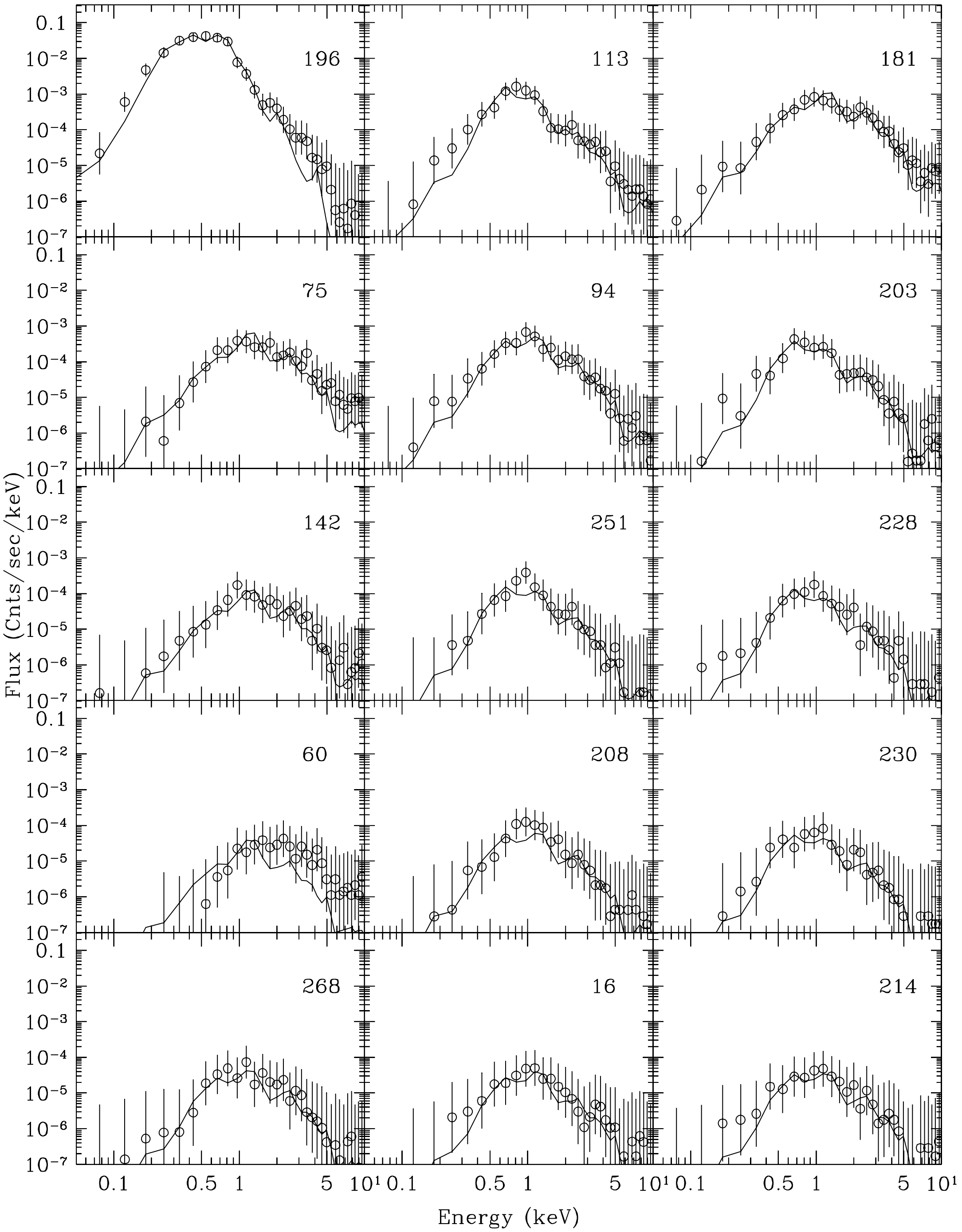

FIG. 4.—Spectra of the 15 brightest sources in our sample. The solid lines show the best model. We used a one plasma temperature model for the brightest source, 196, a known O star, and two plasma temperature models for the rest of the sample. Source 196 was not included in the determination of the conversion factor that leads to L_X.

the X-ray flux. Variable sources with a flarelike light curve are marked with an additional "*f*" in column (13) of Table 1. In Figure 8, we show a selection of light curves of sources of comparable luminosity. In the top panels, we show two light curves with a flare shape; in the middle panels, there are two variable light curves. Finally, in the bottom panels, two constant light curves are plotted. There are six sources that show a possible flare pattern, described as an increase in X-ray flux happening at the end of our observations or a decrease in X-ray flux occurring at the beginning of our observations. Variable sources with a possible flare pattern are marked with an additional "*p*" in column (13) of Table 1. Gagne et al. (1995) detected 10 flaring objects in Orion using *ROSAT* observations, over a sample of 389 X-ray sources (~3% flaring objects); Preibisch & Zinnecker (2002) detected 14 flaring objects in IC 348 using *Chandra* observations over a sample of 215 X-ray sources (~7% flaring objects); we detected a comparable fraction, about 8% flaring sources (5% excluding possible flares).

There are two additional variable sources that show a distinctive pattern of variation, either a steady increase or a steady decrease in X-ray flux. The sources that show this

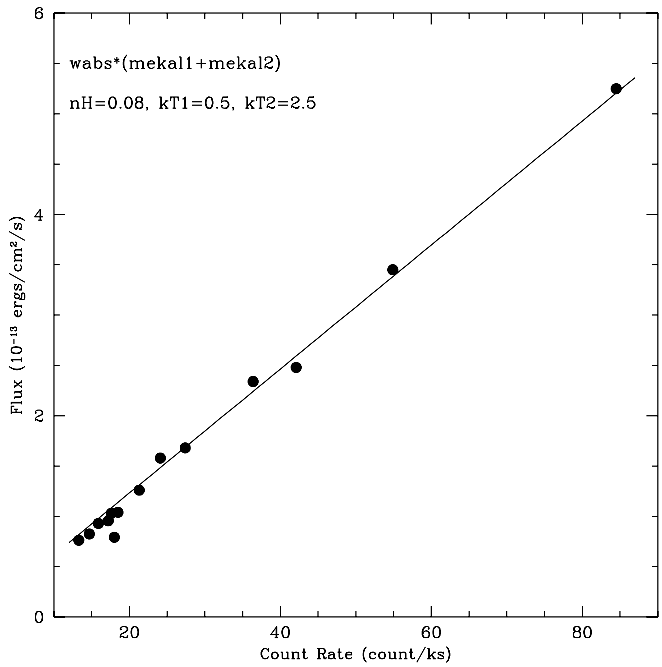

FIG. 5.—CR vs. flux for the 14 bright X-ray sources with two plasma temperature models used to determine a conversion factor. The solid line shows the determined conversion factor of $(6.16 \pm 0.13) \times 10^{-15}$ ergs cm^{-2} s^{-1})/(counts ks^{-1}).

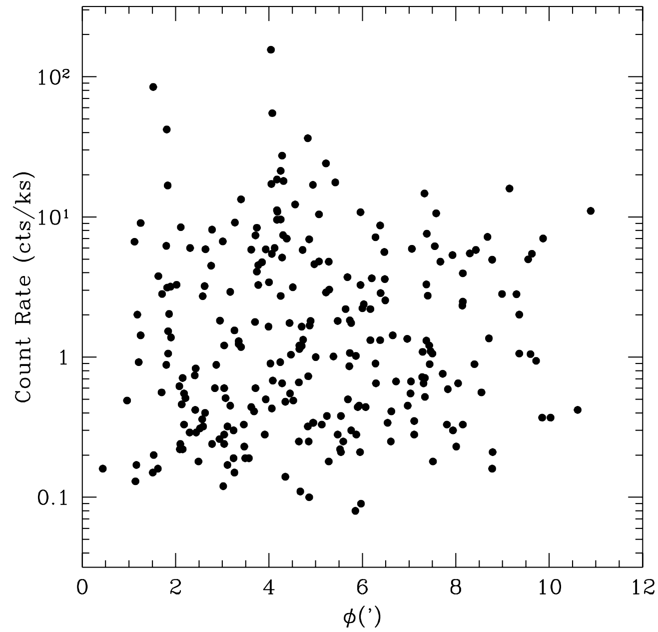

FIG. 6.—CR of detected X-ray sources as a function of the off-axis angle (ϕ). The limiting CR of our observations varies with ϕ, since the PSF of the *Chandra* observations varies across the field of view.

pattern are 75 (R 2752) and 181 (R 3245); they are marked with an additional "*s*" in column (13) of Table 1, and their light curves are shown in Figure 9. The amount of variation in these two cases is about a factor of 10 in about 10 hr. A similar pattern is observed in the light curves of three X-ray IC 348 sources determined by Preibisch & Zinnecker (2002) using *Chandra* observations. They mention that those light curves may be explained by rotational variability, as described by Stelzer et al. (1999), who present a model of rotational modulation of X-ray flares in three T Tauri stars and Algol. The amplitude of the variations modeled by Stelzer et al. (1999) vary from a factor of 2.5 to a factor of 20, depending on the strength of the X-ray flare. Although both X-ray sources 181 and 75 have optical counterparts, only 181 (R 3245) has an observed period of 1.21 days (29 hr) from Makidon et al. (2004). If the light curve of 181 can be understood by rotational modulation of X-ray flares, then the observed decay time ($\sim$11 hr) should be less than half of the stellar period. Therefore, the period implied by the X-ray light curve should be greater than 22 hr, which is consistent with the optical observations.

TABLE 3
COMPARISON OF FLUX CONVERSION FACTORS

Conversion Factor [10^{-15} (ergs cm^{-2} s^{-1})/(counts ks^{-1})]	Reference
5.58	1
7.6–11.9	2
8.04	3
6.88	4
8.46–12.1	5
6.16	6

REFERENCES.—(1) Krishnamurthi et al. 2001; (2) Harnden et al. 2001; (3) Feigelson et al. 2002; (4) Getman et al. 2002; (5) Damiani et al. 2003; (6) this work.

4. DISCUSSION

4.1. *Description of the Optical/Infrared Catalog*

We correlated the X-ray sources with a catalog of stars in NGC 2264; see Table 4. We constructed the catalog by combining our original *UBVRI* survey from Rebull et al.

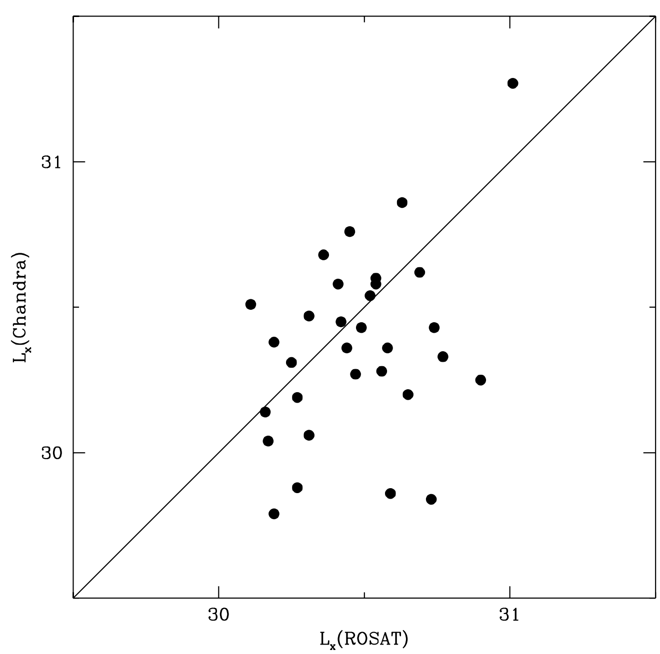

FIG. 7.—Our X-ray luminosities (from *Chandra*) compared with the ones from Flaccomio et al. (2000; from *ROSAT*). The solid line represents the equality of both measurements. Our observations are well-matched to those of Flaccomio et al. (2000).

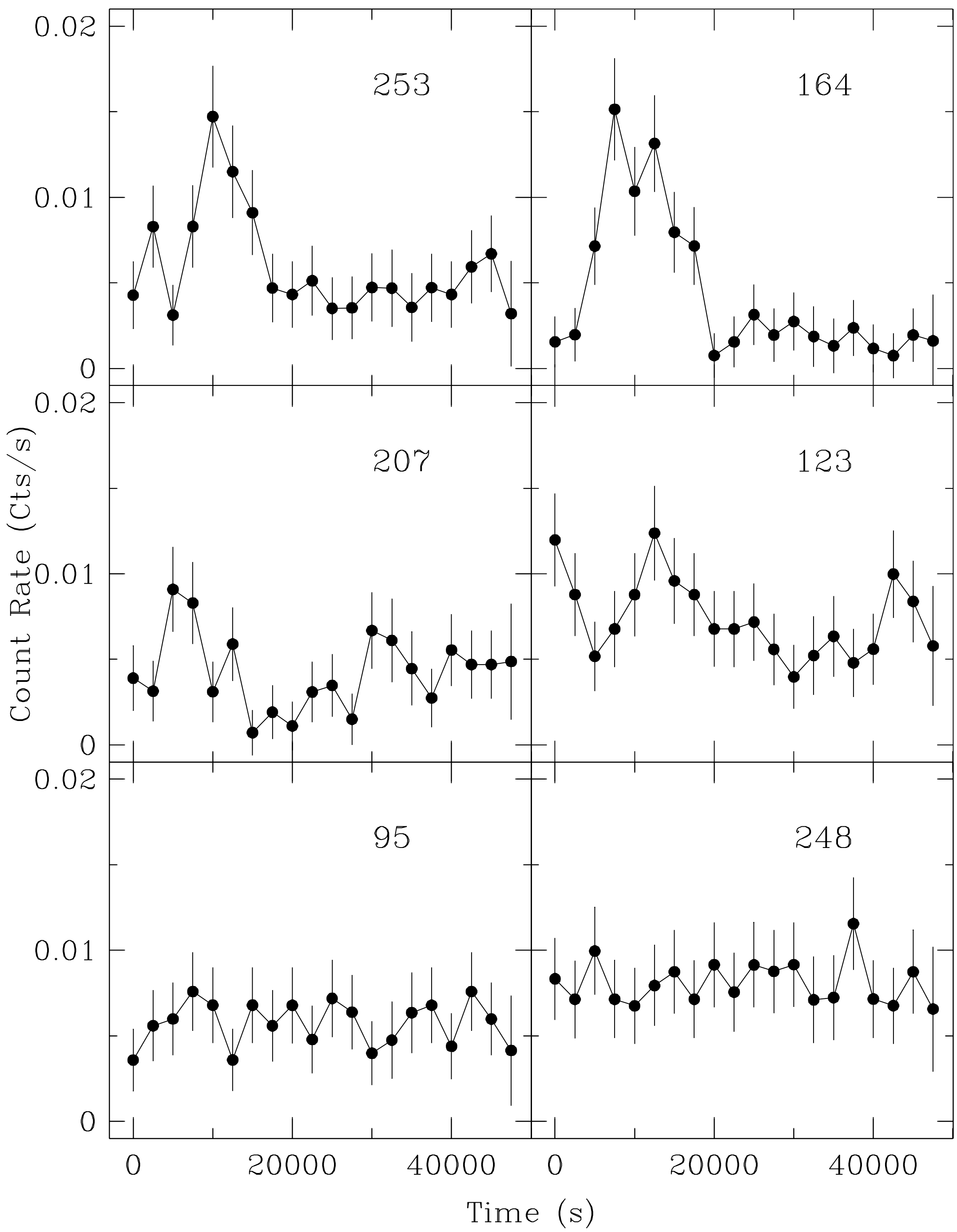

Fig. 8.—Examples of light curves for six X-ray sources of comparable luminosity from our sample. *Top*: Two sources with flarelike light curves. *Middle*: Two variable sources. *Bottom*: Two constant sources. There are 41 variable sources in our sample of 263 X-ray objects; 14 of them show a flarelike light curve.

(2002; "R" names) with other published catalogs. If optical photometry and/or spectral types were not available in Rebull et al. (2002), we took photometry from Park et al. (2000), Flaccomio et al. (1999), or Sung et al. (1997), in that order, augmented by 15 spectral types from the SIMBAD database. All of the *JHK* photometry comes from the Two Micron All Sky Survey (2MASS), with the exception of a handful of stars slightly fainter than the 2MASS limit; those *JHK* values come from Rebull et al. (2002).

We included several other catalogs primarily to keep track of commonly used nomenclature; see Table 5. Herbig (1954), updated by Marcy (1980), lists spectral types and is the origin of the "LkHa" nomenclature; Walker (1956) provides spectral types, membership probabilities, and the commonly used Walker (or "W") names; Ogura (1984) conducted an Hα survey to identify young stars and provides some spectral types; and Vasilevskis et al. (1965) and Herbig & Bell (1988) are the origins of the "VSB" and "HBC" names, respectively. Flaccomio et al. (2000) conducted a *ROSAT* survey of this cluster, and we included these data in our catalog as well (see § 3.2 above). Flaccomio et al. (2000) *ROSAT* sources are named as "FX." Because we are also interested in rotational information (for our future work), we included in our catalog periods from Makidon et al. (2004) and Kearns & Herbst

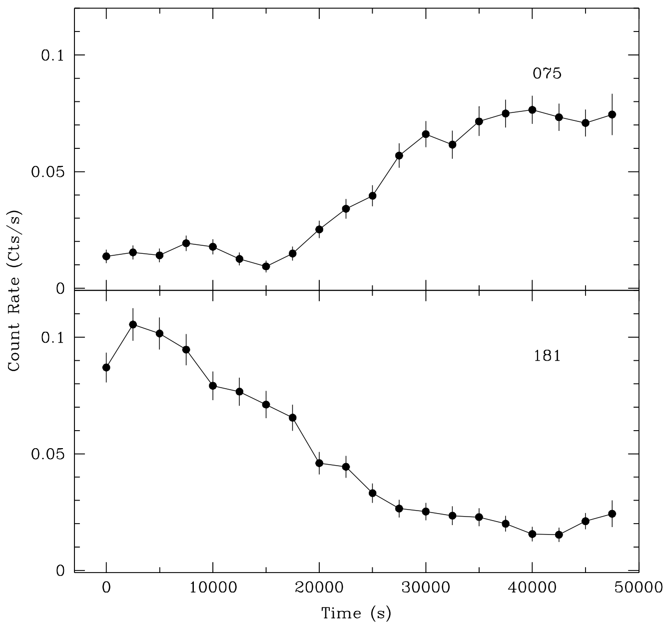

FIG. 9.—Light curves for three X-ray sources that show a steady increase or decrease of flux in their light curves. The amount of variation is about a factor of 10 over about 10 hr.

(1998), as well as projected rotational velocities ($v \sin i$) from McNamara (1990), Soderblom et al. (1999), and Hamilton et al. (2003).

We found that 213 (81%) of our 263 X-ray sources have optical and/or infrared counterparts (108 [41%] have spectral types and 44 [17%] have known periods). Those 213 sources and their corresponding optical and/or infrared photometry are listed in Table 4. Most, but probably not all, of these 213 stars are likely to be members of NGC 2264. Other names of the sources given by the different catalogs used in our compilation are listed in Table 5.

There are 747 stars in our optical/infrared catalog with J, H, and K photometry and with positions inside the field of view of the *Chandra* observations. Among those 747 stars, 199 (27%) have X-ray *Chandra* counterparts. Figure 10 shows a J magnitude histogram of all the 747 stars with J, H, and K photometry and positions inside the *Chandra* field (*solid line*) and the histogram of the 199 X-ray *Chandra* counterparts (*dotted line*). The completeness limit of the infrared sample is essentially that of 2MASS. We can see in Figure 10 that our infrared sample goes deeper than the sample of stars with X-ray counterparts. A similar behavior is seen in the optical sample histogram. This means that all of the X-ray sources should have been matched to sources in our optical/infrared catalog if they are associated with stars earlier than M0 at the distance of NGC 2264. There are 51 X-ray sources that do not have optical or infrared counterparts. Based on the limiting magnitude of our optical catalog ($V \sim 19$ mag), the X-ray–to–optical flux ratio, f_X/f_V, of the sources with only X-ray detection is greater than about $10^{-2.5}$. This means that these sources could be either M stars or extragalactic objects (Stocke et al. 1991). NGC 2264 is located 2° above the Galactic plane, roughly toward the direction of the anticenter. Therefore, most of the M stars should be foreground, and hence detected by 2MASS. Considering the presence of a dark cloud behind NGC 2264, the detection of background M stars in X-rays is unlikely. Source counts in the Chandra South and North Deep Field (Rosati et al. 2002; Brandt et al. 2001) predict the presence of about 100 active galactic nuclei (AGNs) in the ACIS field of view at the flux limit of our observations. Thus, we believe that the most likely explanation is that the 51 objects detected only in X-rays are active galaxies.

4.2. *Color-Color Diagram*

In Figure 11, we have plotted the $J-H$, $H-K$ color-color diagram of all the infrared sources in the field of view of our *Chandra* observation. Most of the X-ray sources with infrared colors are located near the locus of the classical T Tauri (CTT) stars (Meyer et al. 1997). There are two X-ray sources that do not follow the position of the rest of the sources, 161 and S Mon (196). They are marked in the color-color diagram with their X-ray identification numbers. S Mon (see § 4.5.1) is an O star; its position in Figure 11 is correct in $H-K$, but its 2MASS J magnitude is suspect and can be explained by contamination from a nearby diffraction spike. The second source, 161, is a field galaxy (see § 4.5.3).

4.3. *Color-Magnitude Diagrams*

There are 686 stars in our optical/infrared catalog with I_C and V photometry and with positions inside the field of view of the *Chandra* observations. Among those 686 stars, 201 have X-ray *Chandra* counterparts. In Figure 12, we have plotted $(V-I_C)$-M_{I_C} color-magnitude diagrams of the optical sources in the field of view of our *Chandra* observations. The dereddened $V-I_C$ color and the absolute magnitude M_{I_C} were obtained assuming an average extinction of $A_V = 0.41$ and dereddening relationships from Fitzpatrick (1999) and Mathis (1990).

In both panels, we have also plotted isochrones from D'Antona & Mazzitelli (1998), as a reference. The dashed line

TABLE 4
OPTICAL/INFRARED SOURCES WITH X-RAY COUNTERPARTS

Name	R.A. (J2000.0)	Decl. (J2000.0)	X-Ray ID	U (mag)	B (mag)	V (mag)	R (mag)	I_C (mag)	J (mag)	H (mag)	K (mag)
R1817............	6 40 10.00	9 53 41.19	1	18.47	18.36	16.93	16.00	14.94	13.53	12.94	12.73
R2065............	6 40 18.52	9 44 18.73	6	19.65	19.09	17.50	16.51	15.48	14.06	13.40	13.15
R2066............	6 40 18.53	9 52 05.73	8	. . .	20.28	18.94	17.94	16.15	14.55	13.89	13.65
R2093............	6 40 19.37	9 48 29.83	9	18.03	17.38	15.90	15.00	13.99	12.59	11.99	11.89
R2137............	6 40 20.87	9 44 11.29	12	. . .	21.94	20.51	. . .	18.06	16.32	15.84	15.22

NOTE.—Table 4 is presented in its entirety in the electronic edition of the Astronomical Journal. A portion is shown here for guidance regarding its form and content.
[a] Photometry from 2MASS Extended Source Catalog.
[b] Photometry contaminated by a diffraction spike.
[c] Photometry contaminated by a saturated column.

TABLE 5

Cross Identification of Sources with Optical/Infrared Counterparts

X-Ray ID	R Name[a]	Sung Name[b]	2MASS Name	Other Names[c]
1	R1817	...	2MASS J06400993+0953415	...
6	R2065	Sung 1487	2MASS J06401846+0944188	...
8	R2066	...	2MASS J06401847+0952060	...
9	R2093	Sung 68	2MASS J06401930+0948299	...
12	R2137	Sung 1526	2MASS J06402081+0944114	...

Note.—Table 5 is presented in its entirety in the electronic edition of the Astronomical Journal. A portion is shown here for guidance regarding its form and content.

[a] Rebull et al. 2002.

[b] Sung et al. 1997.

[c] (Ogura) Ogura 1984; (Walker) Walker 1956; (VSB) Vasilevskis et al. 1965; (FX) Flaccomio et al. 2000; (HBC) Herbig & Bell 1988; (Herbig) Herbig 1954.

corresponds to $M_{I_C} = 8.75$ mag, which is the lower limit for a low-mass star rotating at the saturation level ($L_X/L_{bol} = -3$) with $L_X = 28.5$ (limit luminosity of our X-ray sample). This means that the most slowly rotating stars with optical counterparts should be detected by our X-ray sample. For comparison, the corresponding line from the *ROSAT* Flaccomio et al. (2000) study would be at $M_{I_C} = 5$ mag.

Most of our X-ray sources are younger than 3×10^6 yr at the distance of NGC 2264, and furthermore the X-ray sources are heavily concentrated toward the youngest isochrones with respect to the general population. All the sources with M_{I_C} brighter than 0.1 mag have $L_X/L_{bol} < 10^{-4}$. Most of those sources have spectral types earlier than A0 (see Fig. 12, *right*). There are five X-ray sources that appear to be much older than 10^7 yr, of which one of them (12) is not a member of NGC 2264, two of them (146 and 273) lack proper motion membership information, and two of them (132 and 259) are probably members (using preliminary membership information as discussed in Rebull et al. 2002). Unfortunately, the optical and infrared photometry of source 259 is unreliable because it is contaminated by a saturated column from a nearby bright star. Source 132 is classified as an M0 star. There are four sources that are located above the 10^5 yr old isochrone, of which two of them (75 and 136) are not members of NGC 2264, one of them (60) lacks proper motion membership information, but it is an A0 star, and one of them (279) is probably a member (using preliminary membership information as discussed in Rebull et al. 2002). Source 279 is classified as a K5 star. We have dereddened sources 279 and 132, using the intrinsic $J-H$, $H-K$, and $R-I_C$ colors of stars of their respective spectral types. For source 279, we derive a A_V value of 5.7 mag and for source 132, A_V is about 3.0 mag. The locations of sources 279 and 132 are indicated along with

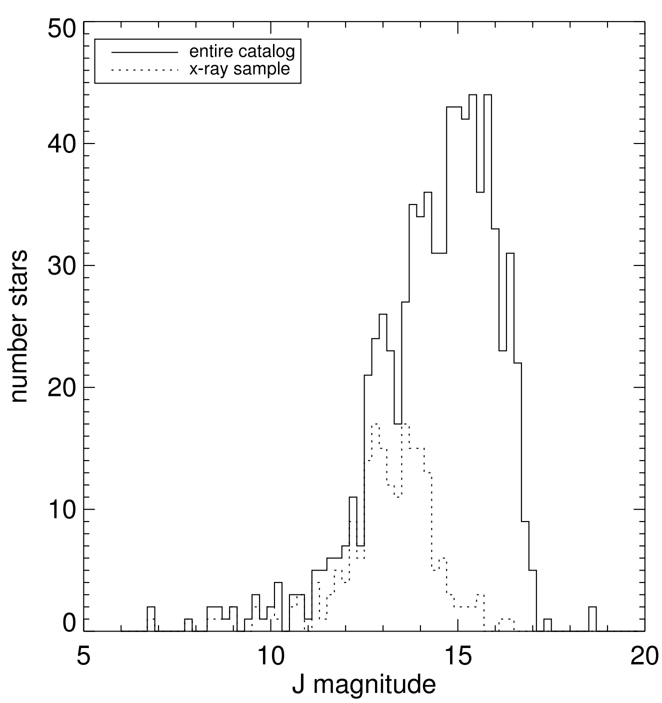

Fig. 10.—*J*-magnitude histogram of all the sources with *J*, *H*, and *K* magnitudes in our *Chandra* field. The solid line corresponds to all the sources, and the dotted line corresponds to all the sources with X-ray counterparts. All the X-ray sources should have been matched to sources in our catalog if they are associated with stars earlier than M0 at the distance of NGC 2264.

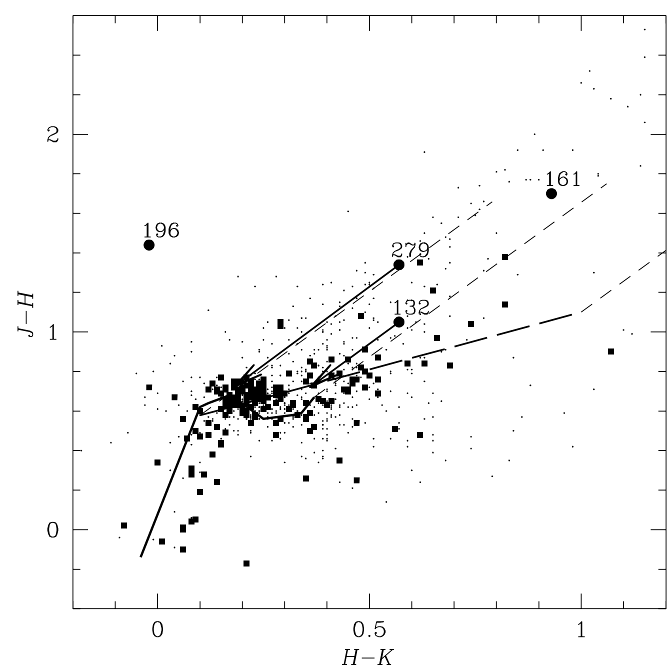

Fig. 11.—Observed infrared color-color diagram of sources located in the field of the ACIS camera showing stars with X-ray counterparts (*squares*), and stars without X-ray counterparts (*dots*). The lines mark the location of main-sequence colors (*thick line*), the locus of CTTs from Meyer et al. (1997) (*dotted line*), and the reddening vectors (*dashed lines*; the length corresponds to $A_V = 10$ mag. Source 196 is an O star with a suspect *J* magnitude, and source 161 is a galaxy; see text. Sources 279 and 132 are also discussed in Fig. 12.

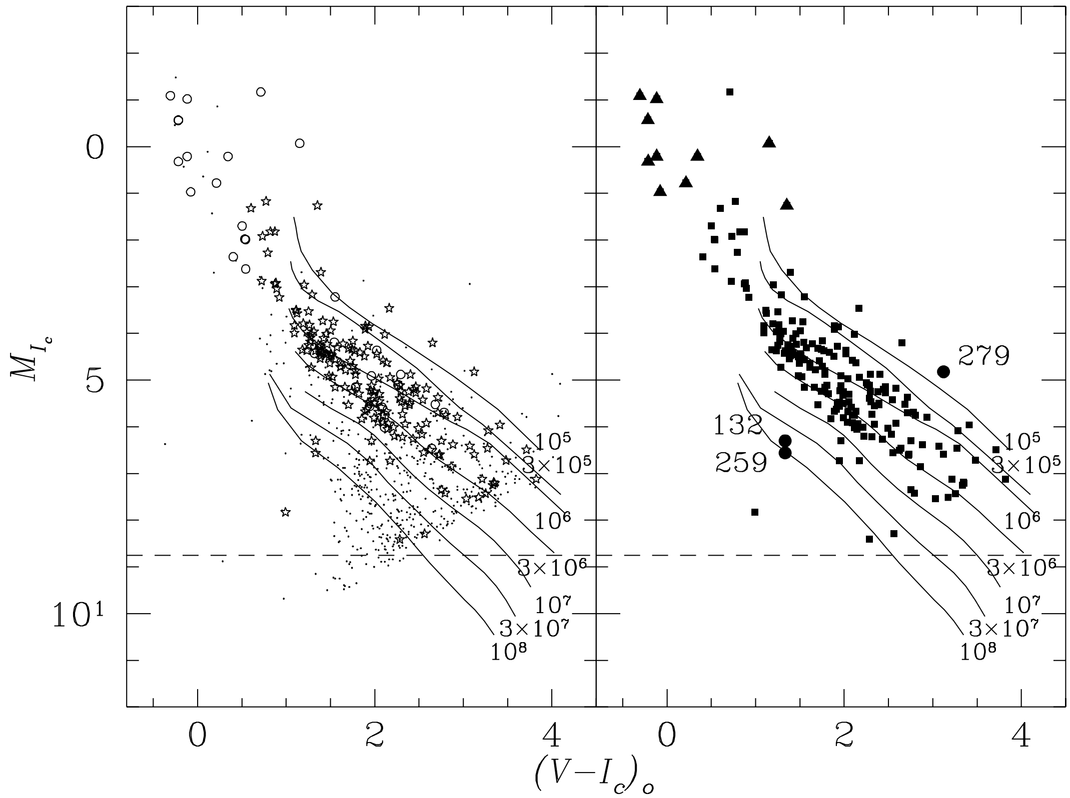

FIG. 12.—Dereddened optical color-magnitude diagrams of sources located in the field of the ACIS camera. *Left*: Positions are shown for stars with X-ray counterparts and $L_X/L_{\rm bol} < 10^{-4}$ (*open circles*), sources with X-ray counterparts and $L_X/L_{\rm bol} < 10^{-4}$ (*stars*), and stars without X-ray counterparts (*filled circles*). *Right*: Only optical sources with X-ray counterparts are plotted. Early-type stars are marked with triangles and sources discussed in the text are marked with circles and their respective X-ray numbers. The dashed line corresponds to $M_{I_C} = 8.5$ mag, which is the lower limit for a low-mass star rotating at the saturation level. The solid lines denote isochrones from D'Antona & Mazzitelli (1998). Most of our X-ray sources are less than 3 Myr old, and they are clearly younger than the general population.

their dereddened positions in Figure 11. The dereddened colors of source 279 are consistent with the colors of a K star, similar to its spectral type, and the dereddened colors of source 132 fall in the locus of CTT stars. In Figure 13, we have plotted the $(J-K)$–M_K color-magnitude diagram of all the infrared sources with X-ray counterparts, with isochrones from D'Antona & Mazzitelli (1998). The location of sources 279 and 132 is indicated along with their dereddened positions. It is possible that these two objects are the youngest and most embedded of our X-ray sources. The unusual optical colors of source 132 could be explained by scattered light from an edge-on disk.

4.4. *Upper Limits*

There are 16 stars for which rotation and spectral type information exist in our optical/infrared catalog, but for which no X-ray counterpart was found. In order to allow us to use these stars in the next paper, we determined upper limits for their X-ray luminosity in the following way. We extracted the counts with an $R_{\rm ext}$ equal to the 95% encircled energy radius. We computed the background counts in the same way as for our detected sources. We used the Bayesian statistics method from Kraft et al. (1991) to determine the net count upper limit to a confidence level of 95%. Then, we computed $f_{\rm PSF}$ and $t_{\rm eff}$ in the same manner as our detected sources, to determine the upper limit for the count rate. The upper limit for the X-ray flux was determined using our derived conversion factor, and the upper limit for the X-ray luminosity was computed assuming a distance to NGC 2264 of 760 pc (Sung et al. 1997). The upper limit results are listed in Table 6.

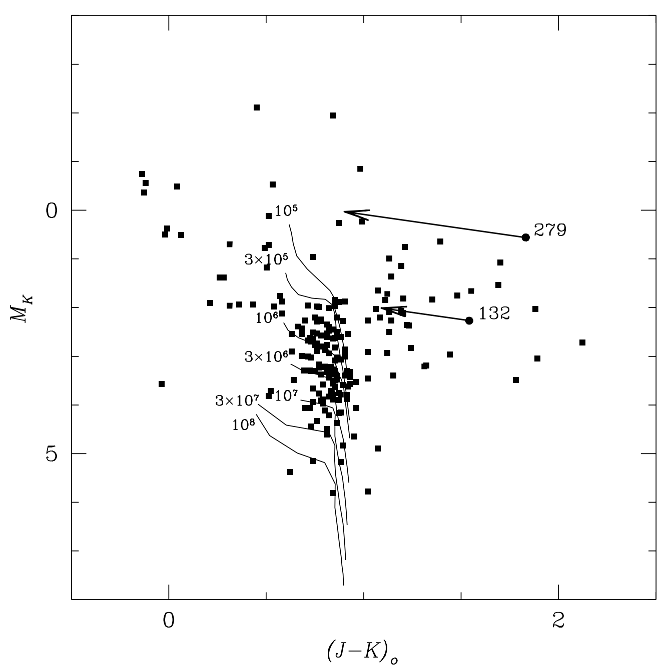

FIG. 13.—Dereddened infrared color-magnitude diagram of sources located in the field of the ACIS camera. Only infrared sources with X-ray counterparts are plotted. Sources 132 and 279 are marked with their X-ray number, and their dereddened positions are marked with arrows. The solid lines denote isochrones from D'Antona & Mazzitelli (1998). Sources 279 and 132 are likely to be the youngest and most embedded of our X-ray sources; the unusual optical colors of source 132 could be explained by scattered light from an edge-on disk.

TABLE 6

Upper Limits for Some Optical/Infrared Stars in the Chandra Field

R Name	Sung Name	2MASS Name	Other Names	Counts	CR (counts ks^{-1})	Flux (10^{-13} ergs cm^{-2} s^{-1})	log L_X [log (ergs s^{-1})]
R 2772	Sung 153	2MASS 06404102+0947577	...	<4.11	<0.0955	<0.0056	<28.61
R 2898	Sung 173	2MASS 06404464+0948021	Walker 90, V590 Mon, HBC 219, VSB 62	<3.00	<0.0703	<0.0041	<28.48
R 2982	Sung 2066	2MASS 06404729+0947274	...	<12.63	<0.3940	<0.0231	<29.22
R 2491	Sung 1760	2MASS 06403200+094935	...	<3.00	<0.1794	<0.0105	<28.88
	...	...	V590 Mon, HBC 219, Herbig 25	<4.11	<0.0962	<0.0056	<28.61
R 2792	Sung 159	2MASS 06404156+0955174	VSB 56	<3.00	<0.1984	<0.0116	<28.93
	...	...	LN Mon, HBC 215, Herbig 21	<4.82	<0.1193	<0.0070	<28.71
R 3167	Sung 2178	2MASS 06405413+0948434	...	<4.11	<0.0944	<0.0055	<28.60
R 3216	Sung 2206	2MASS 06405573+0946456	...	<3.82	<0.0903	<0.0053	<28.58
	...	...	LR Mon, HBC 220, Herbig 27	<4.11	<0.1816	<0.0106	<28.89
R 2972	Sung 2056	2MASS 06404694+0955036	...	<7.24	<0.1697	<0.0099	<28.86
R 3022	Sung 195	MASS 06404888+0951444	Walker 100, HD 261841, VSB 72	<7.40	<0.1677	<0.0098	<28.85
R 3041	Sung 196	2MASS 06404953+0953230	Walker 104, VSB 74	<6.78	<0.1561	<0.0092	<28.82
R 3073	Sung 2125	2MASS 06405033+0954158	...	<4.11	<0.0958	<0.0056	<28.61
R 3110..........	Sung 209	2MASS 06405155+0951494	Walker 109, HD 261878, VSB 79	<5.82	<0.1328	<0.0078	<28.75
	...	...	FX 67, VSB 245	<3.94	<0.0926	<0.0054	<28.60

4.5. *Other Interesting Objects*

4.5.1. *S Mon*

X-ray source 196 is associated with S Mon, an O7 V star. The X-ray spectrum of S Mon is well fitted by two plasma temperatures 0.18 and 0.57 keV, but nearly 80% of the total X-ray flux comes from the 0.18 keV component. We derive a $\log(L_X/L_{bol}) = -6.78$, which is in good agreement with the canonical value of $\log(L_X/L_{bol}) \sim -7$ observed in O stars (Chlebowski et al. 1989; Cassinelli et al. 1994). Berghofer, Schmitt, & Cassinelli (1996) provide a catalog of OB stars observed in the *ROSAT* All-Sky Survey, which includes S Mon. They derive (from hardness ratios) an X-ray plasma temperature of 0.23 keV and $\log(L_X/L_{bol}) \sim -6.63$, which are in good agreement with the values we derive considering the differences in the applied techniques (spectral fitting vs. hardness ratios). The X-ray emission mechanism for early-type stars is thought to be very different from the magnetic reconnection flares that generate the X-rays in low-mass young stars. Models predict that the X-ray emission of hot stars comes from shocks formed within a radiatively driven wind (Lucy & White 1980; Lucy 1982), producing X-rays of about 0.5 keV. The shocks may be formed by line-forced instabilities (Owocki et al. 1988; Feldmeier et al. 1997). Evidence coming from grating X-ray spectroscopy suggests that magnetically confined hot plasma near the surface of the star may be important in some early-type stars that show an unusually hard X-ray spectrum (plasma temperature higher than 2 keV) and narrow X-ray emission lines (e.g., Babel & Montmerle 1997; Cohen, Cassinelli, & Waldron 1997, 2003). The lack of a hard component in the X-ray spectrum of S Mon may suggest that its X-ray emission is likely produced by shocks within the radiatively driven stellar wind.

4.5.2. *Walker 90*

Walker 90 is an early-type emission-line star that lies below the zero-age main sequence in the V, $B-V$ color-magnitude diagram (Strom et al. 1971), suggesting very nonselective extinction. Sitko et al. (1984) confirmed the existence of anomalous circumstellar dust extinction, which they explained by a graphite-silicate mixture with larger grains than those present in the diffuse interstellar medium. Walker 90 is in our *Chandra* field, but no X-ray source was detected at its position. An upper limit for its X-ray luminosity is provided in Table 6.

4.5.3. *A Relatively Bright Active Galaxy toward Our Chandra Field*

Our X-ray source 161 is coincident in position and has similar morphology to the extended infrared source 2MASX J06405286+0948570. The J, H, and K magnitudes from the 2MASS extended source catalog are listed in Table 4. This source is also a known radio source, with a flux of 6.45 mJy beam^{-1} at 3.6 cm (Rodríguez & Reipurth 1994) and a flux of 61.9 mJy at 20 cm (Condon et al. 1998). Given its radio and X-ray emission, we conclude that source 161 is a radio-quiet AGN (Elvis et al. 1994), seen through the molecular cloud.

5. CONCLUSIONS

We present a catalog of NGC 2264 X-ray sources. The observations were taken with the ACIS-I on board the *Chandra X-Ray Observatory*. The catalog, consisting of 263 sources, includes X-ray luminosity, optical and infrared photometry, and X-ray variability information. We found 41 variable sources, 14 of which have a flarelike light curve, and two of which have a pattern of a steady increase or decrease. From the optical and infrared counterparts of the X-ray sources, we have learned that most of the X-ray sources have colors consistent with CTTs that are younger than 3×10^6 yr.

This catalog of X-ray sources will be used to study the relationship between rotational properties and X-ray characteristics of NGC 2264 stars in Paper II (Rebull et al. 2004). We plan to discuss correlations of L_X/L_{bol} with rotation rate (period and $v \sin i$), disk indicators (I_C-K, $H-K$, $U-V$, and Hα), and mass accretion rates as derived from $U-V$ excess. We will also compare the L_X/L_{bol} values found here with those from other young clusters.

S. V. R. gratefully thanks Jeonghee Rho, Kenji Hamaguchi, Ettore Flaccomio, Peter Freeman. and Scott Wolk for the useful correspondence about X-ray and *Chandra* data processing and analysis. S. V. R. also thanks August Muench, Paul Eskridge, Richard Pogge, Phil Appleton, Mark Lacy, and Dario Fadda for interesting discussions. We thank the anonymous referee for her/his careful review of the manuscript. Financial support for this work was provided by NASA grant GO2-3011X. This research has made extensive use of NASA's Astrophysics Data System Abstract Service, the SIMBAD database, operated at CDS, Strasbourg, France, and the NASA/IPAC Infrared Science Archive, which is operated by the Jet Propulsion Laboratory, California Institute of Technology, under contract with the National Aeronautics and Space Administration. The research described in this paper was partially carried out at the Jet Propulsion Laboratory, California Institute of Technology, under a contract with the National Aeronautics and Space Administration.

REFERENCES

Adams, M. T., Strom, K. M., & Strom, S. E. 1983, ApJS, 53, 893
Babel, J., & Montmerle, T. 1997, ApJ, 485, L29
Berghofer, T. W., Schmitt, J. H. M. M., & Cassinelli, J. P. 1996, A&AS, 118, 481
Brandt, W. N., et al. 2001, AJ, 122, 2810
Cassinelli, J. P., Cohen, D. H., MacFarlane, J. J., Sanders, W. T., & Welsh, B. Y. 1994, ApJ, 421, 705
Chlebowski, T., Harnden, F. R., & Sciortino, S. 1989, ApJ, 341, 427
Cohen, D. H., Cassinelli, J. P., & Waldron, W. L. 1997, ApJ, 488, 397
Cohen, D. H., de Messieres, G. E., MacFarlane, J. J., Miller, N. A., Cassinelli, J. P., Owocki, S. P., & Liedahl, D. A. 2003, ApJ, 586, 495
Condon, J. J., Cotton, W. D., Greisen, E. W., Yin, Q. F., Perley, R. A., Taylor, G. B., & Broderick, J. J. 1998, AJ, 115, 1693
Damiani, F., Flaccomio, E., Micela, G., Sciortino, S., Harnden, F. R., Jr., Murray, S. S., Wolk, S. J., & Jeffries, R. D. 2003, ApJ, 588, 1009
D'Antona, F., & Mazzitelli, I. 1998, ASP Conf. Ser. 134, Brown Dwarfs and Extrasolar Planets, ed. R. Rebolo, E. L. Martin, M. R. Zapatero Osorio, (San Francisco: ASP), 442
Elvis, M., Wilkes, B. J., McDowell, J. C., Green, R. F., Bechtold, J., Willner, S. P., Oey, M. S., Polomski, E., & Cutri, R. 1994, ApJS, 95, 1
Feigelson, E. D., Bross, P., Gaffney, J. A., Garmire, G., Hillenbrand, L. A., Pravdo, S. H., Townsley, L., & Tsuboi, Y. 2002, ApJ, 574, 258
Feigelson, E. D., Gaffney, J. A., Garmire, G., Hillenbrand, L. A., & Townsley, L. 2003, ApJ, 584, 911
Feldmeier, A., Puls, J., & Pauldrach, A. W. A. 1997, A&A, 322, 878
Fitzpatrick, E. L. 1999, PASP, 111, 63
Flaccomio, E., Micela, G., & Sciortino, S. 2003, A&A, 402, 277
Flaccomio, E., Micela, G., Sciortino, S., Damiani, F., Favata, F., Harnden, F. R., & Schachter, J. 2000, A&A, 355, 651

Flaccomio, E., Micela, G., Sciortino, S, Favata, F., Corbally, C., & Tomaney, A. 1999, A&A, 345, 521
Freeman, P. E., Kashyap, V., Rosner, R., & Lamb, D. Q. 2002, ApJS, 138, 185
Gagne, M., Caillault, J.-P., & Stauffer, J. R. 1995, ApJ, 445, 280
Getman, K. V., Feigelson, E. D., Townsley, L., Bally, J., Lada, C. J., & Reipurth, B. 2002, ApJ, 575, 354
Hamilton, C. M., Herbst, W., Mundt, R., Bailer-Jones, C. A. L., & Johns-Krull, C. M. 2003, ApJ, 591, L45
Harnden, F. R., Jr., et al. 2001, ApJ, 547, L141
Herbig, G. H. 1954, ApJ, 119, 483
Herbig, G. H., & Bell, K. R. 1988, Lick Obs. Bull., No. 1111, 1
Hillenbrand, L. 1997, AJ, 113, 1733
Jeffries, R. D., Totten, E. J., & James, D. J. 2000, MNRAS, 316, 950
Kaastra, J. S. 1992, An X-Ray Spectral Code for Optically Thin Plasmas, Version 2 (Internal SRON-Leiden Rep.; Leiden: SRON)
Kearns, K., & Herbst, W. 1998, AJ, 116, 261
Kraft, R. P., Burrows, D. N., & Nousek, J. A. 1991, ApJ, 374, 344
Krishnamurthi, A., Reynolds, C. S., Linsky, J. L., Martín, E., & Gagne, M. 2001, AJ, 121, 337
Lada, C. J., Young, E. T., & Greene, T. P. 1993, ApJ, 408, 471
Liedahl, D. A., Osterheld, A. L., & Goldstein, W. H. 1995, ApJ, 438, L115
Lucy, L. B. 1982, ApJ, 255, L286
Lucy, L. B., & White, R. L. 1980, ApJ, 241, L300
Makidon, R. B., Rebull, L., Strom, S., Adams, M., & Patten, B. 2004, AJ, 127, 2228
Marcy, G. W. 1980, AJ, 85, 230
Mathis, J. S. 1990, ARA&A, 28, 37
McNamara, B. 1990, ApJ, 350, 348
Mewe, R., Gronenschild, E. H. B. M., & van den Oord, G. H. J. 1985, A&AS, 62, 197
Mewe, R., Lemen, J. R., & van den Oord, G. H. J. 1986, A&AS, 65, 511
Meyer, M. R., Calvet, N. , & Hillenbrand, L. A. 1997, AJ, 114, 288
Morrison, R., & McCammon, D. 1983, ApJ, 270, 119
Ogura, K. 1984, PASJ, 36, 139
Owocki, S. P., Castor, J. I., & Rybicki, G. B. 1988, ApJ, 335, 914
Park, B.-G., et al. 2000, AJ, 120, 894
Patten, B., Simon, T., Strom, S., & Strom, K. 1994, in ASP Conf. Ser. 64, Cool Stars, Stellar Systems, and the Sun, ed. J.-P. Caillault (San Francisco: ASP), 125
Pizzolato, N., Maggio, A., Micela, G., Sciortino, S., & Ventura, P. 2003, A&A, 397, 147
Preibisch, T., & Zinnecker, H. 2002, AJ, 123, 1613
Rebull, L. M., et al. 2002, AJ, 123, 1528
———. 2004, in preparation
Reid, I. N., et al. 1991, PASP, 103, 661
Rodríguez, L. F., & Reipurth, B. 1994, A&A, 281, 882
Rosati, P., et al. 2002, ApJ, 566, 667
Simon, T., Cash, W., & Snow, T. P., Jr. 1985, ApJ, 293, 542
Sitko, M. L., Simon, T., & Meade, M. R. 1984, PASP, 96, 54
Soderblom, D. R., King, J. R., Siess, L., Jones, B. F., & Fischer, D. 1999, AJ, 118, 1301
Stauffer, J. R., Balachandran, S. C., Krishnamurthi, A., Pinsonneault, M., Terndrup, D. M., & Stern, R. A. 1997, ApJ, 475, 604
Stelzer, B., Neuhauser, R., Casanova, S., & Montmerle, T. 1999, A&A, 344, 154
Stocke, J. T., Morris, S. L., Gioia, I. M., Maccacaro, T., Schild, R., Wolter, A., Fleming, T. A., & Henry, J. P. 1991, ApJS, 76, 813
Strom, K. M., Strom, S. E., & Yost, J. 1971, ApJ, 165, 479
Sung, H., Bessell, M., & Lee, S.-W. 1997, AJ, 114, 2644
Townsley, L. K., Broos, P. S., Garmire, G. P., & Nousek, J. A. 2000, ApJ, 534, L139
Vasilevskis, S., et al. 1965, AJ, 70, 797
Walker, M. F. 1956, ApJS, 2, 365
Weisskopf, M. C., Brinkman, B., Canizares, C., Garmire, G., Murray, S., & Van Speybroeck, L. P. 2002, PASP, 114, 1